



# Experimental and Modeling Optimization of Strontium Adsorption on Microbial Nanocellulose, Eco-friendly Approach

Rofaida S. Abd Elkader<sup>1</sup> · Mokhtar K. Mohamed<sup>2</sup> · Yasmeen A. Hasanien<sup>3</sup> · Eman M. Kandeel<sup>2</sup>

Received: 18 February 2023 / Accepted: 22 May 2023 / Published online: 13 June 2023  
© The Author(s) 2023

## Abstract

Green synthesized cellulose nanocrystals (CNCs) was prepared using *Neurospora intermedia*, characterized, and used to remove Strontium ions ( $\text{Sr}^{2+}$ ) from an aqueous solution with high efficiency. The characterization of CNCs was performed using a UV-Vis Spectrophotometer, Dynamic Light Scattering (DLS), Zeta Potential (ZP), Fourier Transform Infrared Spectroscopy (FTIR), X-Ray Diffraction (XRD), and Scanning Electron Microscopy (SEM) mapping, EDX elemental analysis and BET surface analyzer. In this study, Response Surface Methodology (RSM) based on Box-Behnken Design (BBD) was successfully applied for the first time to optimize the dynamic adsorption conditions for the maximum removal of  $\text{Sr}^{2+}$  ions from aqueous solutions using CNCs as adsorbent. The effects of parameters, such as initial concentration of  $\text{Sr}^{2+}$  (50–500 ppm), adsorbent dosage (0.05–0.2 g/50ml), and contact time (15–120 min.) on removal efficiency were investigated. A mathematical model was studied to predict the removal performance. The significance and adequacy of the model were surveyed using the analysis of variance (ANOVA). The results showed that the second-order polynomial model is suitable for the prediction removal of  $\text{Sr}^{2+}$  with regression coefficient ( $R^2 = 97.41\%$ ). The highest sorption capacity value of  $\text{Sr}^{2+}$  was obtained (281.89 mg/g) at the adsorbent dosage of 0.05 g/50 ml, contact time of 120 min., and the pollutant ( $\text{Sr}^{2+}$ ) concentration of 275 ppm.

**Keywords** Strontium · Nanocellulose · Adsorption · RSM · Bioremediation · Optimization

## List of Abbreviations

ANOVA Analysis of variance  
BBD Box-Behnken Design  
BET Brunauer-Emmett-Teller  
BJH Barrett-Joyner-Halenda

BLAST Basic Local Alignment Search Tool  
CI Crystallinity Index  
CNCs Cellulose nanocrystals  
DLS Dynamic light scattering  
EDX Energy Dispersive X-Ray  
ELS Electrophoretic Light Scattering  
FTIR Fourier transform infrared spectroscopy  
FWHM Full width at half maximum of peak  
MCC Microcrystalline cellulose  
MeV Mega electron volt  
PDA Potato Dextrose Agar  
rpm Round per minute  
RSM Response surface methodology  
SEM Scanning electron microscopy  
XRD X ray defraction  
ZP Zeta Potential

✉ Mokhtar K. Mohamed  
Kamal.mokhtar@yahoo.com

Rofaida S. Abd Elkader  
rofaidamicro@gmail.com

Yasmeen A. Hasanien  
yasmeen21485@gmail.com

Eman M. Kandeel  
eman\_abdelhadi@yahoo.com

<sup>1</sup> Soil and Water Research Department, Nuclear Research Center, Egyptian Atomic Energy Authority, Cairo, Egypt

<sup>2</sup> Radiation Protection and Safety Department, Hot Labs Center, Egyptian Atomic Energy Authority, Cairo, Egypt

<sup>3</sup> Plant Research Department, Nuclear Research Center, Egyptian Atomic Energy Authority, Cairo, Egypt

## Introduction

The development of nuclear industries has led to the release of large amounts of radioactive wastewater into the environment. Radio-strontium is a significant radionuclide in the low-level radioactive waste from nuclear power reactors [1]. The seriousness of the strontium is that isotope  $^{90}\text{Sr}$  has a half-life of (28.8 years) and is a pure beta emitter with a 0.546 MeV energy [2]. Because of its chemical resemblance to calcium (Ca), strontium (Sr) penetrates the human body and integrates into bones just like calcium does [3]. Leukemia, bone sarcoma, and other long-term difficulties can result from the radioactive material  $^{90}\text{Sr}$  entering bone [4]. Both stable and radioactive Sr can be dissolved in water due to its high solubility [5, 6]. Most of the stable Sr input to rivers or groundwater is from the weathering of celestite-rich limestone or rocks, while the radioactive Sr in the water usually originates from nuclear power plants or weapons factories [7, 8]. Moreover, due to inadequate strontium-bearing waste treatment, a high  $\text{Sr}^{2+}$  concentration can be found in surface water, industrial wastewater, and seawater [9]. Therefore, it is crucial to remove  $\text{Sr}^{2+}$  from wastewater.

The remediation of  $\text{Sr}^{2+}$  from wastewater has been proposed using traditional technologies, including reverse osmosis, electrodialysis, adsorption, flocculation, ultrafiltration, and chemical precipitation [10–13]. However, the most used technique is adsorption because of its high removal efficiency, design flexibility, and low cost [14, 15]. Adsorption is an accumulation process of a gas or liquid onto a solid phase called an adsorbent [16, 17]. Contaminants can adhere to the surface of an adsorbent using different physical forces [18].

Recently, nanocellulose has attracted attention due to its increased specific surface area, outstanding mechanical characteristics, and great biocompatibility [19, 20]. It has become a novel class of biobased adsorbent with prospective uses in environmental remediation against a wide range of contaminants because of its wide range of potential functionalization, reactivity, processability, biodegradability, and reversibility [17, 21]. Interestingly, nanocellulose may adsorb 40 times its weight in substances, according to Jin, Kettunen [22]. Cellulose nanocrystals (CNCs) were utilized as adsorbents to remove many heavy metals, such as Cr (VI), Ni (II), and Cd (II), from an aqueous solution [23–25].

The physical and chemical properties of cellulose nanocrystals can vary depending on the extraction method and the source of cellulose. Physical, chemical, or microbiological processing was used to extract nanocellulose from their source materials [26]. An alternate method for producing nanocellulose that depends mainly on the principles of green chemistry is to utilize microbes instead of hazardous chemicals for green/sustainable development. During

synthesis, biomolecules like enzymes and proteins released by the microbial biomass may act as capping and reducing agents [27, 28].

Reviewing the literature revealed that no study, in which the efficiency of CNCs for the  $\text{Sr}^{2+}$  removal from wastewater was investigated, was established. In this regard, the aim of this investigation was to extend the performance of microbial CNCs for  $\text{Sr}^{2+}$  removal from an aqueous solution. Therefore, it is essential to evaluate the effect of process variables on removal efficiency. The response surface methodology (RSM) was employed to evaluate variables and the effect of their interaction and predict the optimum condition at a minimized number of experiments [29–31]. Therefore, the experimental and analytical methods using RSM were better developed than the one variable at a time method [32, 33].

The novelty is focused on using myogenic CNCs as a green biosorbent for  $\text{Sr}^{2+}$  removal with high efficiency. The resulting CNCs were characterized to assess the characteristic feature of the used biosorbent.

This study also intends to evaluate the effects of process variables, such as initial concentration, adsorbent dosage, and contact time, in order to identify the optimum conditions of the  $\text{Sr}^{2+}$  removal process using the Box-Behnken Design (BBD). Furthermore, the statistical results and diagnostic checking test were assessed using the analysis of variance (ANOVA). Finally, CNCs were compared with other adsorbents to find out its efficiency.

## Materials and Methods

### Materials

Microcrystalline cellulose (MCC) with high purity, (20 microne) from Sigma Alderich company, No. S3504.

### Microbial Strains

The tested isolate was previously isolated using nylon net bag techniques, selected from 37 isolates for testing on cellulase enzyme production, identified at the AUMC in Assiut, Egypt, and sequenced. The recovered sequences were then deposited in Gen Bank with the accession number MZ724159 as in prior work performed by Helal, Khalil [34]. This isolate was identified as *Neurospora intermedia* (AUMC 14,359). With the help of Basic Local Alignment Search Tool (BLAST) algorithms, the sequence was compared to other sequences in the Gen Bank database.

## Microbiological Media

Potato Dextrose Agar (PDA) [35] g/l: Potato slices, 250; Glucose, 20; Agar, 20. Czapek-Dox's agar medium was prepared according to Dox [36] with the following contents: (Sucrose 30.0); (NaNO<sub>3</sub> 2.0); (KH<sub>2</sub>PO<sub>4</sub> 1.0); (MgSO<sub>4</sub>·7H<sub>2</sub>O 0.5); (KCl 0.5); (FeSO<sub>4</sub>·5H<sub>2</sub>O 0.001). The pH of the medium was adjusted to 7.0 by applying (0.1–2 N) HCl or NaOH.

## Microbial Synthesis of CNCs Adsorbent

By inoculating a spore suspension (~3 × 10<sup>5</sup> spores/ml), a 24-hour inoculum of the fungus *Neurospora intermedia* (AUMC 14,359) strains was grown in potato dextrose broth. In a 250 ml conical flask at 25 or 30 °C with stirring, the ideal concentration (2.5%) of inoculum was introduced to Czapek-Dox Agar medium containing microcrystalline cellulose (MCC) as the only carbon source (150 rpm). After fermentation, the broth was subjected to relatively different centrifugal forces to optimize the sedimentation of all particles larger than 1 μm in size [37–39].

## Characterization of CNCs Adsorbent

### UV-Vis Spectrophotometer

The prepared solution of the obtained CNCs was initially analyzed on a UV-Vis spectrophotometer. The absorbance of cellulose was measured from 190 to 800 nm using UV / Vis spectroscopy (JENWAY-UK- model 6850) at 220/110 VAC, 50/60 Hz, 120 VA placed in the Chemical Department/ Atomic Energy Authority.

### DLS and ZP Analysis

The suspension of CNCs was prepared as described above using *Neurospora intermedia* from MCC. Approximately 1.5 ml of filtrate containing CNCs was taken and placed in a glass tube in the refrigerator until analysis. To avoid agglomeration, the sample was subjected to sonication for 15 min before analysis. Where the sonication involves the use of high-frequency sound waves to disperse the nanoparticles in the solution [40].

The particle size distribution, polydispersity index and surface charge of the suspended CNCs were measured using (Zetasizer Nano-ZS, Malvern, UK) at Egypt Petroleum Research Institute (EPRI), EPIR-Nanotechnology Center. This instrument uses a design that allows both multi-angle particle size analysis using DLS and low-angle zeta potential analysis using electrophoretic light scattering (ELS) [41].

## FTIR Analysis

The suspension of CNCs was made in the manner described above. As a control, fungal strains were cultivated on Potato Dextrose Broth (PDB) without substrate. Samples and control were incubated at 30 °C for 7 days. After the incubation period, it was filtrated with filter paper to prepare samples for FTIR analysis.

FTIR spectra were measured using (FTIR, IRAffinity-1 spectrophotometer, Shimadzu, Japan) and recorded at 400–4000 cm<sup>-1</sup> at the Egyptian Petroleum Research Institute, Nanotechnology Center.

## XRD Analysis

Since CNCs that are suspended in liquid have a tendency to agglomerate, it is difficult to obtain optimal sample compositions for XRD analysis [42]. Therefore, for XRD analysis, the CNCs were prepared by drying the suspension containing the CNCs in a 45 °C oven for at least 48 h and scraping off the formed CNCs. X-Ray Diffraction (XRD) analysis was used to identify the size and crystal type of the produced CNCs (XRD-6000, Shimadzu Scientific Instruments, Japan). The CNCs were scanned between 2θ = 5° and 90° at a step rate of 0.2 s/step at 25 °C, λ = 0.1540 nm. The following equation was used to estimate the dried cellulose's crystallinity index (CI) [43]:

$$CI (\%) = \frac{A_{\text{crystalline}}}{A_{\text{amorphous}} + A_{\text{crystalline}}} \times 100 \quad (1)$$

Where: A<sub>crystalline</sub> is the region under the sample curve, and A<sub>amorphous</sub> is the region under the amorphous curve. Scherrer's equation was used to determine the cellulose crystal size [44]:

$$\text{Crystalsize (nm)} = \frac{k\lambda}{\beta \cos\theta} \quad (2)$$

Where: λ (X-ray wavelength) = 0.1540 Å, k is the (correction factor) = 0.91, θ = diffraction angle (radians), and β = full width at half maximum of peak (FWHM).

## SEM-EDX Analysis

SEM analysis (SEM, ZEISS, EVO-MA10, Germany) was used to investigate surface morphology, boundary size and the distribution of the synthesized CNCs around the prepared filtrate and the starting materials (MCC). To study the elemental composition, and the purity of elements founded in the synthesized materials, Energy Dispersive X-Ray (EDX), BRUKER, Nano GmbH, D-12,489, 410-M,

Germany was conducted. Finally, the SEM/EDX mapping technique was used to assess the distribution of each element by giving them distinct colors.

### BET Analysis

Using a Quantachrome NOVA 4000e, measurements of adsorption and desorption were carried out (Quantachrome Instruments, Boynton Beach, FL, USA). Nitrogen (77.350 K) was used as the test gas in a surface area and pore size analyzer. Before measurement, all samples underwent a 24-hour vacuum degassing period at room temperature. The specific surface area from gas adsorption was calculated using the Brunauer-Emmett-Teller (BET) methodology. The Barrett-Joyner-Halenda (BJH) model, applied to volumetric desorption isotherms, was used to estimate the pore-size distributions for each sample.

#### Strontium (Sr<sup>2+</sup>) adsorption studies.

Through aqueous solutions of Sr<sup>2+</sup> ions, the adsorption capacity of CNCs for Sr<sup>2+</sup> was examined. SrCl<sub>2</sub> was dissolved in distilled water to create the standard solutions of Sr<sup>2+</sup>. The adsorption capacity MCC of CNCs for Sr<sup>2+</sup> was investigated through aqueous solutions of strontium ions. The standard solutions of Sr<sup>2+</sup> were formed in distilled water by dissolving SrCl<sub>2</sub>. Adsorption experimentations were carried out through batch technique at constant conditions: (temperature 25 ± 3 °C, stirring rate 120 rpm, and pH 6 ± 0.5). The effects of adsorbent weight, initial Sr<sup>2+</sup> concentration, and contact time on the removal efficiency of Sr<sup>2+</sup> onto CNCs were optimized by RSM.

The desired concentration of Sr<sup>2+</sup> and final volume (20 ml) was prepared; then, the pH was adjusted at 6 ± 0.5 before sterilization. After cooling, the desired weight of CNCs adsorbent was added. All flasks were incubated at optimum conditions. At the end of the incubation period, the adsorbent was discarded by filtration. The supernatant was collected and centrifuged to determine the adsorbed Sr<sup>2+</sup> ions as follows:

$$\text{Removal percentage (R\%)} = \frac{C_0 - C_e}{C_0} \times 100 \quad (3)$$

$$\text{Adsorption capacity (q}_e\text{)} = \frac{(C_0 - C_e)V}{m} \quad (4)$$

**Table 1** Studied variables with Box-Behnken design codes and levels

Variables	symbol	Coded and actual values			Unit
		-1	0	+1	
Contact time	A	15	67.5	120	min.
Initial Sr <sup>2+</sup> conc.	B	50	275	500	g/L
Adsorbent (CNCs) wt.	C	0.050	0.125	0.2	g

Conc. Concentration, wt. weight, min. minute, g gram

where  $q_e$  is the amount of Sr<sup>2+</sup> adsorbed by a unit mass of an adsorbent (mg g<sup>-1</sup>), and  $C_0$  and  $C_e$  are the concentrations of Sr<sup>2+</sup> ions in aqueous solution (mg) before and after adsorption, respectively.  $V$  and  $m$  are the volumes of solution (L) and dry weight (g) of CNCs adsorbent, respectively.

### Experimental Design (RSM/BBD)

In contrast to traditional statistical analysis, the Design of Experiments (DOE) was used to identify the optimal values of experimental parameters and their interaction. The reduced experimental runs help DOE to save energy, time, and material use [26, 45]. A collection of mathematical and statistical tools called RSM was developed as a DOE method and was helpful for creating, enhancing, and optimizing processes [46, 47]. As a subset of RSM, BBD was frequently utilized because of its various benefits over other techniques, including the ability to model and optimize factors quickly, simply, and with a minimal number of experiments [48].

The maximum capacity for Sr<sup>2+</sup> adsorption on CNCs adsorbent was evaluated using three levels for each of the three selected independent parameters, contact time (A), the initial concentration of Sr<sup>2+</sup> (B), and adsorbent weight (C) according to (BBD). The lowest and highest levels of the variables were contact time 15 and 120 min, the initial concentration of Sr<sup>2+</sup> 50 and 500 ppm, and adsorbent weight 0.05 and 0.2 g illustrated in Table 1. A second order polynomial equation was fitted to connect the relationship between the independent factors and the response (sorption capacity) in order to determine the optimal point. The following was the equation for the three variables:

$$Y = \beta_0 + \beta_1X_1 + \beta_2X_2 + \beta_3X_3 + \beta_{12}X_1X_2 + \beta_{13}X_1X_3 + \beta_{23}X_2X_3 + \beta_{11}X_1^2 + \beta_{22}X_2^2 + \beta_{33}X_3^2 \quad (5)$$

Where  $Y$  is the predicted response;  $\beta_0$  is the constant of model;  $X_1$ ,  $X_2$ , and  $X_3$  are the independent variables;  $\beta_1$ ,  $\beta_2$ , and  $\beta_3$  are the linear coefficients;  $\beta_{12}$ ,  $\beta_{13}$ , and  $\beta_{23}$  are the crossproduct coefficients; and  $\beta_{11}$ ,  $\beta_{22}$ , and  $\beta_{33}$  are the quadratic coefficients. Regression analysis and graphical analysis were performed using Minitab 18. The coefficient of determination  $R^2$  described how well the polynomial model equation fit the data.

## Results and Discussion

### Characterization of CNCs

Nanocellulose was synthesized by *Neurospora intermedia* from microcrystalline cellulose (MCC) as cellulose

substrates. The produced cellulose nanocrystals (CNCs) were recognized and described according to their characteristic features as follows:

### Optical Properties of CNCs

To characterize the optical properties of produced nanocellulose, UV-Vis spectroscopy is a practical and widely used technique [49]. The UV-vis absorption spectrum of nano-sized particles reveals peaks characteristic of the surface plasmon resonance [50]. The UV absorption spectrum from 200 to 400 nm and the visible spectrum from 400 to 700 nm of the cellulose solution were measured. The corresponding results are shown in (Fig. 1a), which shows the absorption spectra at 270 nm for CNCs produced, which is a characteristic band for cellulose. The present data agreed with those obtained by [51, 52], who concluded that the common absorption peak of cellulose was at 270 nm. This result is consistent with the line of previous studies, which indicated

that the absorption spectrum was observed at 275 nm for nanocellulose [53–55].

when the cellulose particle size is reduced of CNCs.

The average size and polydispersity index (PDI) of cellulose nanoparticles were determined by Dynamic Light Scattering (DLS). (Fig. 1b) shows the DLS graph of the CNC solution synthesized by *Neuro intermedia* fungus. The particle size distribution had average diameters of (55.04 nm) with a 97.4% number, and the size distribution profile was between 39 and 82 nm.

The polydispersity index (PDI), developed to define the level of non-uniformity in a nanoparticle size distribution, can also be used to detect the aggregation of nanoparticles [56]. This index, which is also called the heterogeneity index, is dimensionless, and its values fall between 0 and 1, with 0 indicating a highly heterogeneous population and 1 indicating a highly heterogeneous population [57]. It was, therefore, evident that the PDI value (0.61) for the synthesized CNCs showed a mid-range uniformity of a particle size distribution; as this value approached 0, the size distribution

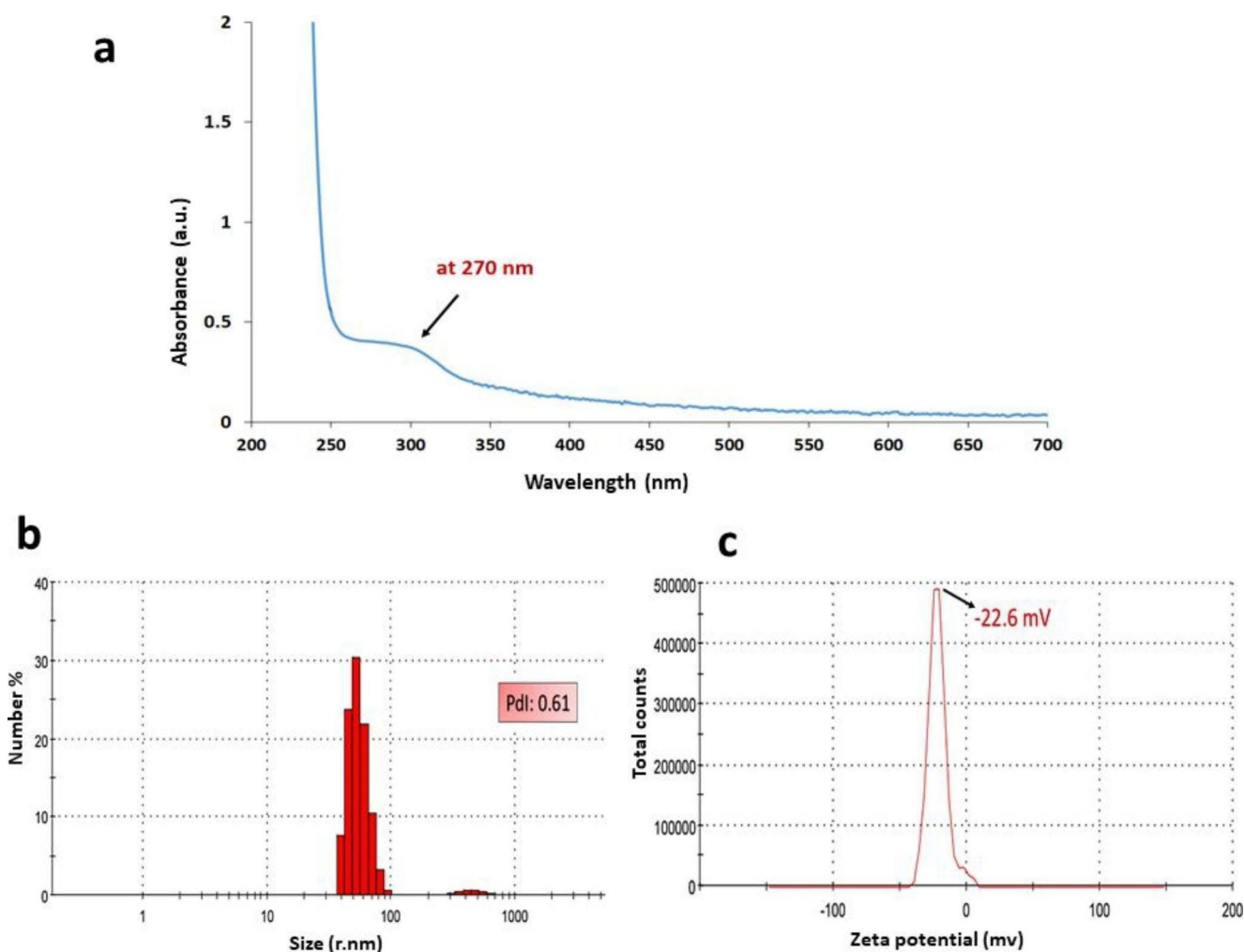


Fig. 1 Characterization of CNCs (a) UV-Vis spectroscopy, (b) DLS analysis, (c) Zeta potential

of the nanoparticles in the nanoparticle suspensions became more homogeneous [58]. When the cellulose particle size is reduced to the nanoscale, the resultant high specific area leads to an improved adsorption capacity [59, 60].

### Surface Charge

A vital method for estimating the surface charge of nanocrystals is the assessment of their zeta potential. This method can be used to evaluate the physical stability of nanosuspensions [57]. It is the charge that forms at a solid surface's contact with its liquid medium; on the other hand, it predicts a colloidal dispersion's long-term stability [61]. The data illustrated in (Fig. 1c) clarified that the average zeta potential value of CNC was  $-22.6$  mV, indicating their stability. Masruchin, Amanda [62] claimed that at a value of  $\pm 30$  mV, the stable zeta potential for suspension in water was attained. Zeta potential levels served as a measure of the stability of NPs, with larger absolute values indicating more stable NPs [57].

### Surface Bonding and Functional Groups

FTIR examination was applied to analyze surface bonding and chemical functional groups present in the prepared sample. The FTIR analysis also investigated the difference between the synthesized CNCs and active metabolites from the cell-free filtrate of the tested isolates, *N. intermedia*.

(Fig. 2a) exhibits the FTIR spectra of the cell-free filtrate of *N. intermedia* and the produced CNC in the range  $400\text{--}4000$   $\text{cm}^{-1}$ . The peak at  $3451.94$   $\text{cm}^{-1}$  for CNC was associated with O-H stretching intramolecular hydrogen bonds for cellulose I. The same peak was observed in the spectra of nanocellulose whiskers, indicating that they both were cellulose I [63]. Bands at  $2922.75$   $\text{cm}^{-1}$  for control,  $2925.60$ , and  $2853.28$   $\text{cm}^{-1}$  for CNCs were assigned to C-H stretching vibration. The peak at  $1641.19$   $\text{cm}^{-1}$  was associated with  $\text{cm}^{-1}$  C=C stretching, characteristic of NC [64]. Peaks at  $1033$   $\text{cm}^{-1}$  for control and  $1167.74$  and  $1114.7$   $\text{cm}^{-1}$  were assigned to medium C-N stretch of aliphatic amines. Additional bands appeared in the spectrum of the synthesized CNCs, possibly as a result of their conjugation. These bands (peak at  $1641.19$   $\text{cm}^{-1}$  were assigned to the N-H bend of 1 amine. The peak at  $2428.04$  and the peak at  $2361.51$   $\text{cm}^{-1}$  were associated with C=C conjugated, the peak at  $2925.60$  and the peak at  $2853.28$   $\text{cm}^{-1}$  were assigned to C-H stretching vibration), the characteristic band at  $1383.73$   $\text{cm}^{-1}$  was associated to CH aliphatic bending group, the peaks at  $1167.74$  and  $1114.7$   $\text{cm}^{-1}$  were assigned to C-N stretch aliphatic amines, the peak at  $833.13$   $\text{cm}^{-1}$  was assigned to strong =C-H bend of alkenes, and the band at  $618.09$   $\text{cm}^{-1}$  was associated with  $\text{--C}\equiv\text{C--H}$ : C-H bend in alkynes.

According to earlier research, these bands were connected to the anhydroglucopyranose unit's deformation, wagging, and twisting behaviors [65]. In the nanocellulose FTIR curve, as compared to the linear FTIR spectrum, there were more peaks and a higher degree of spectrum resolution. There were some peaks between  $600$   $\text{cm}^{-1}$  and  $1100$   $\text{cm}^{-1}$  and other peaks between  $1350$   $\text{cm}^{-1}$  and  $1175$   $\text{cm}^{-1}$ , which showed that the nanocellulose contained sulfonates [66]. The efficacy of nanocellulose as an adsorbent is mostly due to the functionalization of the material, which is illustrated by the abundance of hydroxyl groups on its surface, especially when taken together with its higher adsorption capability [67].

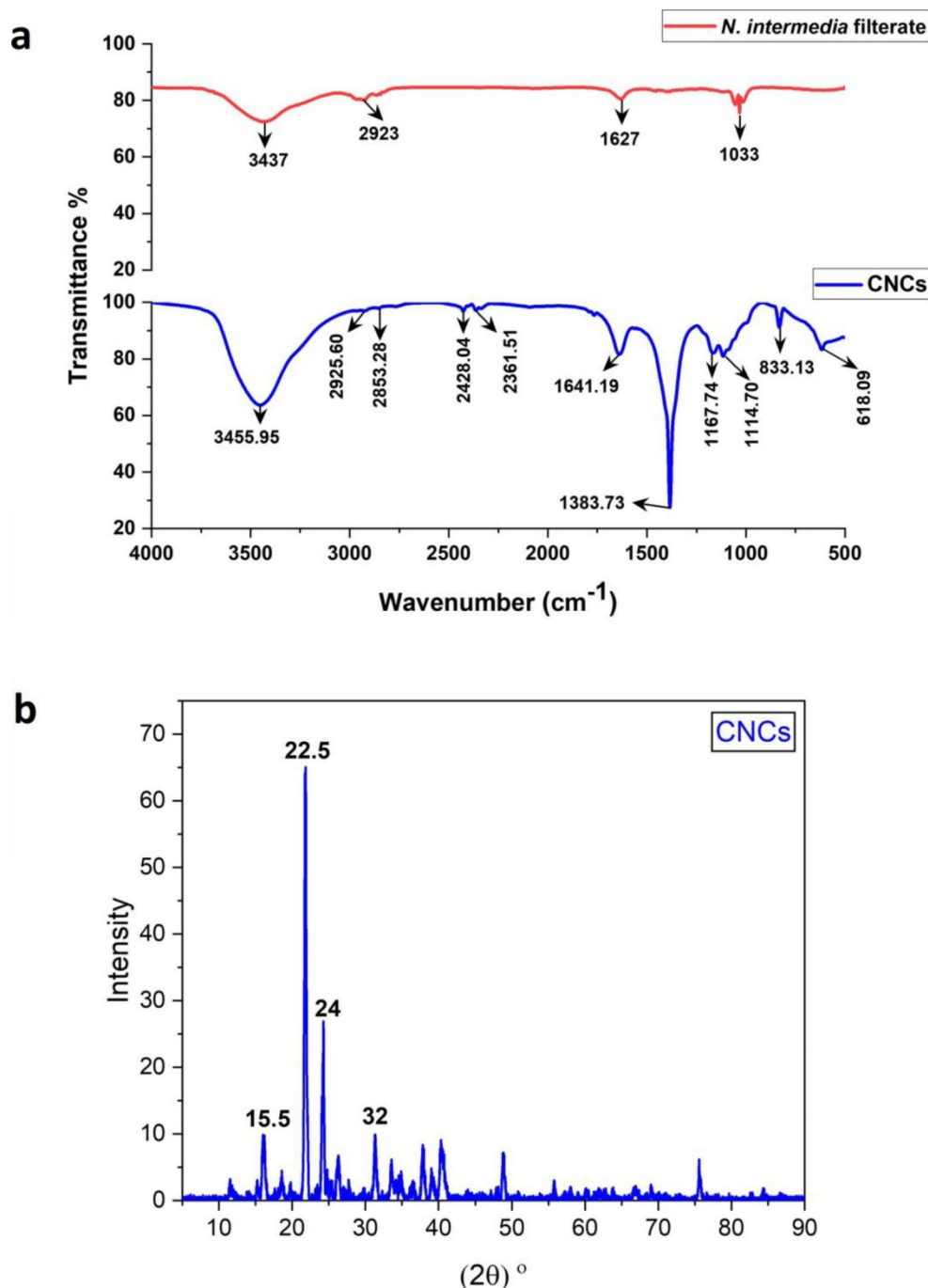
### Crystallography

Crystallography is the investigation of how atoms and molecules are arranged in crystallized solids. A variety of structural characteristics of crystalline samples are examined using the versatile technique of XRD [68]. XRD analysis for CNCs is presented in (Fig. 2b). The XRD pattern findings showed that four different intense peaks were observed at the diffraction angle  $(2\theta) = 15.5^\circ$ ,  $22.5^\circ$ ,  $24^\circ$ , and  $32^\circ$ , in accordance with the nanocrystals of cellulose as reported by different studies [69–71]. The crystallinity index and crystal size of CNCs were 68.09% and 21.76 nm, respectively.

### Surface Morphology and Elemental Analysis

Surface morphology and elemental analysis of the prepared CNCs, and the starting MCC are shown in Fig. 3. SEM is a recommended method for studying surface morphology, particularly the dimensional property. The signals that result from electron sample interactions provide details about the sample, such as its chemical composition and surface morphology (texture) [72]. EDX spectroscopy was employed to analyze the elemental structure, and to validate the prepared samples [73]. It can be recognized from Fig. (3a) that the starting precursor MCC is present as an irregular shape with a hazy, leaf-like structure and is a bright particle when it is regularly in its pure form. EDX study was used to establish the basic structure of the established MCC, which exhibited the main absorption peaks of oxygen and carbon, which are the main elements in the MCC chemical structure. The lack of other elemental peaks and the massive quantity of MCC in the spectra validate the element purity, while Si atoms were found to be in traces during the handling of the sample exhibited in Fig. (3b). On the other hand, for the prepared CNCs, SEM imaging (Fig. 3c) confirms the formation of specific spheroid-shaped bright particles on the surface of the rough filtrate and explains the role of the filtrate in the synthetic way in addition to their role in the stabilization.

**Fig. 2** Characterization of CNCs  
**a)** FTIR spectra of the cell-free filtrate of *N. intermedia* and the synthesized CNCs, **b)** XRD pattern of CNCs synthesized using *N. intermedia*



Finally, the EDX analysis of the prepared CNCs (Fig. 3d) exhibited specific absorption peaks of carbon and oxygen (the main elements in cellulose’s building body). Also, there are some elements like Na, Si, S, Cl, K, Ca, Mg, and N which are suggested to be the main elements present in the synthetic filtrate and the prepared medium.

**Elemental Mapping Analysis and Porosity Measurements**

The elemental mappings of the starting material MCC are displayed in Fig. 4. All images are identified as C, O and Si for MCC. From this figure, it is obvious that C and O are equally distributed without the presence of any other foreign elements except for Si, which is taken from the handling process. Finally, the same situation exists for the synthesized CNCs (Fig. 5), which explains the distribution

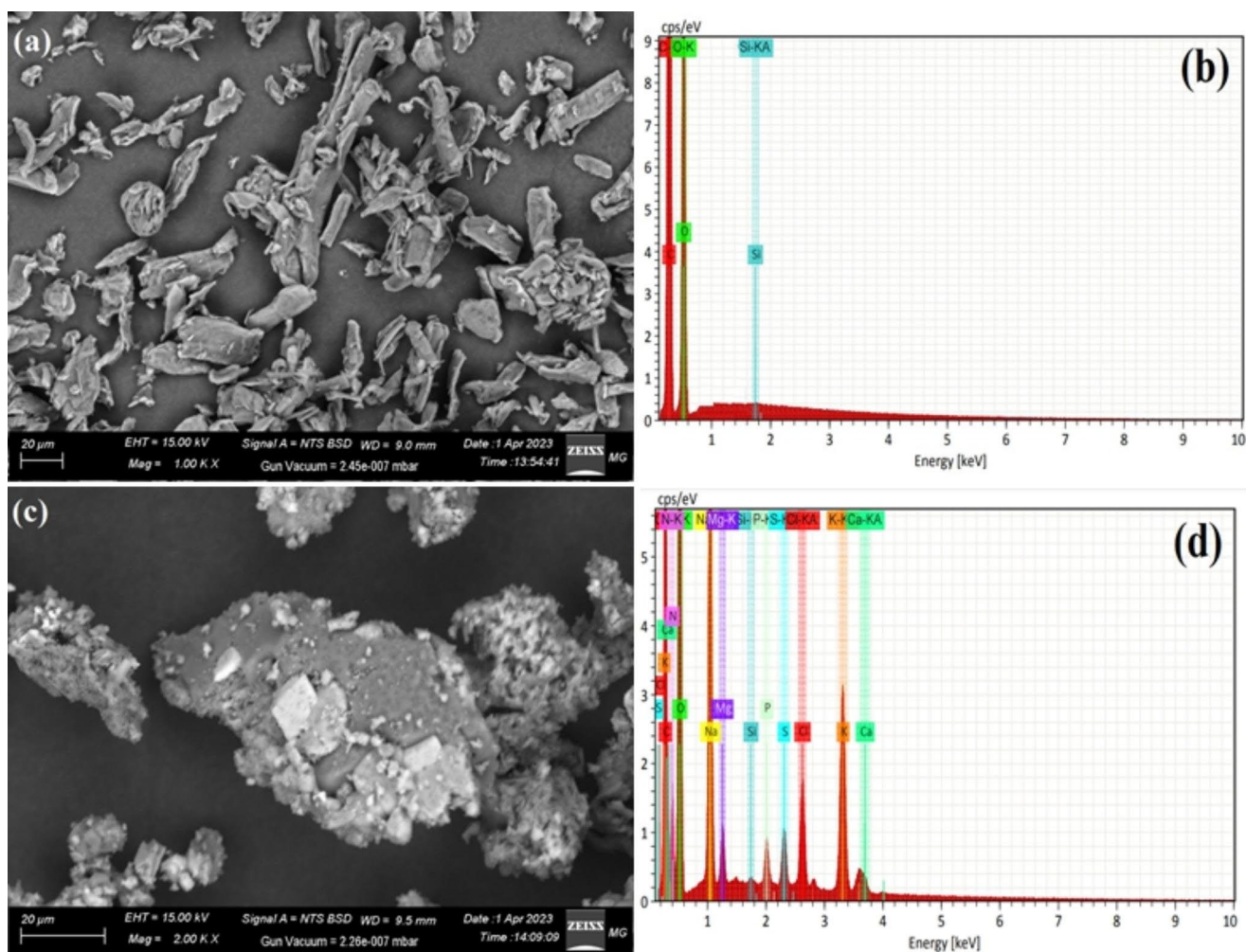


**Fig. 3** Morphological behavior, purity, and elemental analysis for the synthesized CNCs, and the starting material MCC where, (a) SEM for MCC, (b) The corresponding EDX of MCC, (c) SEM for CNCs, and (d) The corresponding EDX of CNCs

of elements that form the CNCs (C, and O) across the filtrate and describes the role of the filtrate in the synthetic approach through the presence of some elements (Na, S, Cl, K, Ca, Mg, and N) normally present in the constituents of the fungal filtrate and the media used.

N<sub>2</sub> adsorption–desorption isotherm was used to analyze the porosity and surface area of CNCs. The surface area was calculated to be 10.48 m<sup>2</sup> g<sup>-1</sup>.

The calculated pore size distribution showed that the average pore size was about 1.7174 nm. On the other hand, pore volume of the prepared CNCs was found to be 3.587 e<sup>-6</sup> cm<sup>3</sup> g<sup>-1</sup>.

### Experimental Design and Optimization

BBD, a statistical and mathematical technique useful for creating models, planning experiments, and examining the interactive effects of numerous independent parameters, was used to investigate the impact of sorption

process parameters on the removal percentage of Sr<sup>2+</sup> onto CNCs.

(Table 2) reports the experimental design and the obtained results. Each experiment was carried out in accordance with the conditions listed in Table 2, and the sorption capacity was calculated. At a constant pH of 6, the sorption capacity ranged from 6.28 to 281.89 mg/g dry weight. At an adsorbent dosage of (0.050 g), a contact time of 120 min, and a Sr<sup>2+</sup> concentration of 275 ppm, the greatest sorption capacity value was attained.

### Analysis of Variance (ANOVA)

Through ANOVA, the significance and adequacy of the models were evaluated [74]. The results for the ANOVA of the response surface quadratic analyses and model terms are summarized in Table 3. As can be seen, the model's *F* value was 16.69, and the probability value of 0.008 (<0.05) showed that this model was significant



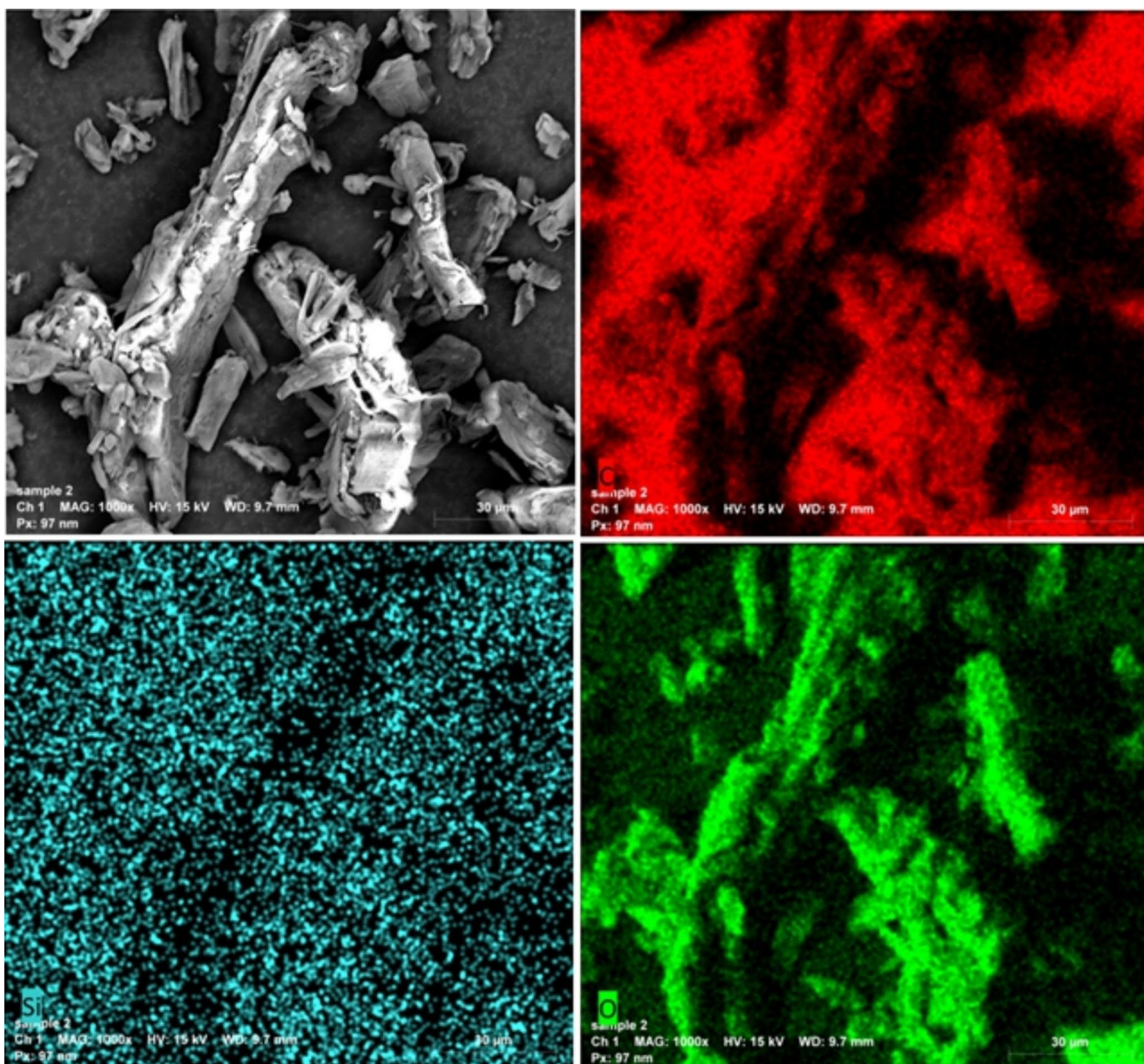


**Fig. 4** SEM/EDX mapping analysis for the starting material MCC

at the 95% confidence level [75]. The higher  $R^2$  value (0.9741) and adjusted  $R^2$  value (0.9157) showed that the quadratic models utilized were highly sufficient in predicting the responses. In addition, the lack of fit (0.006) was insignificant, suggesting that the model was adequate and that there was no need to add higher-order terms to the model under analysis [76].

By evaluating the interaction effect that exist between the selected variables, it was found that all of the 2-way interacted factors (AB, AC, BC), linear variable (C) and square variable ( $B^2$ ) represented a negative significant effect on the response while two linear variables (A, B) and two squared variables ( $A^2$ ,  $C^2$ ) revealed a positive

significant interacted effect on sorption capacity according to  $T$  value results illustrated in Table 3; Fig. 4b. The second-order polynomial equation determined using the model regression analysis could be as the following:

$$\begin{aligned} \text{Sorption Capacity } mg/g \text{ dry wt} = & 136 + 0.36A + 0.670B - \\ & 2599C + 0.00695A^2 - 0.000646B^2 + 10,229C^2 - \\ & 0.00001AB - 7.94AC - 1.36BC \end{aligned} \tag{6}$$

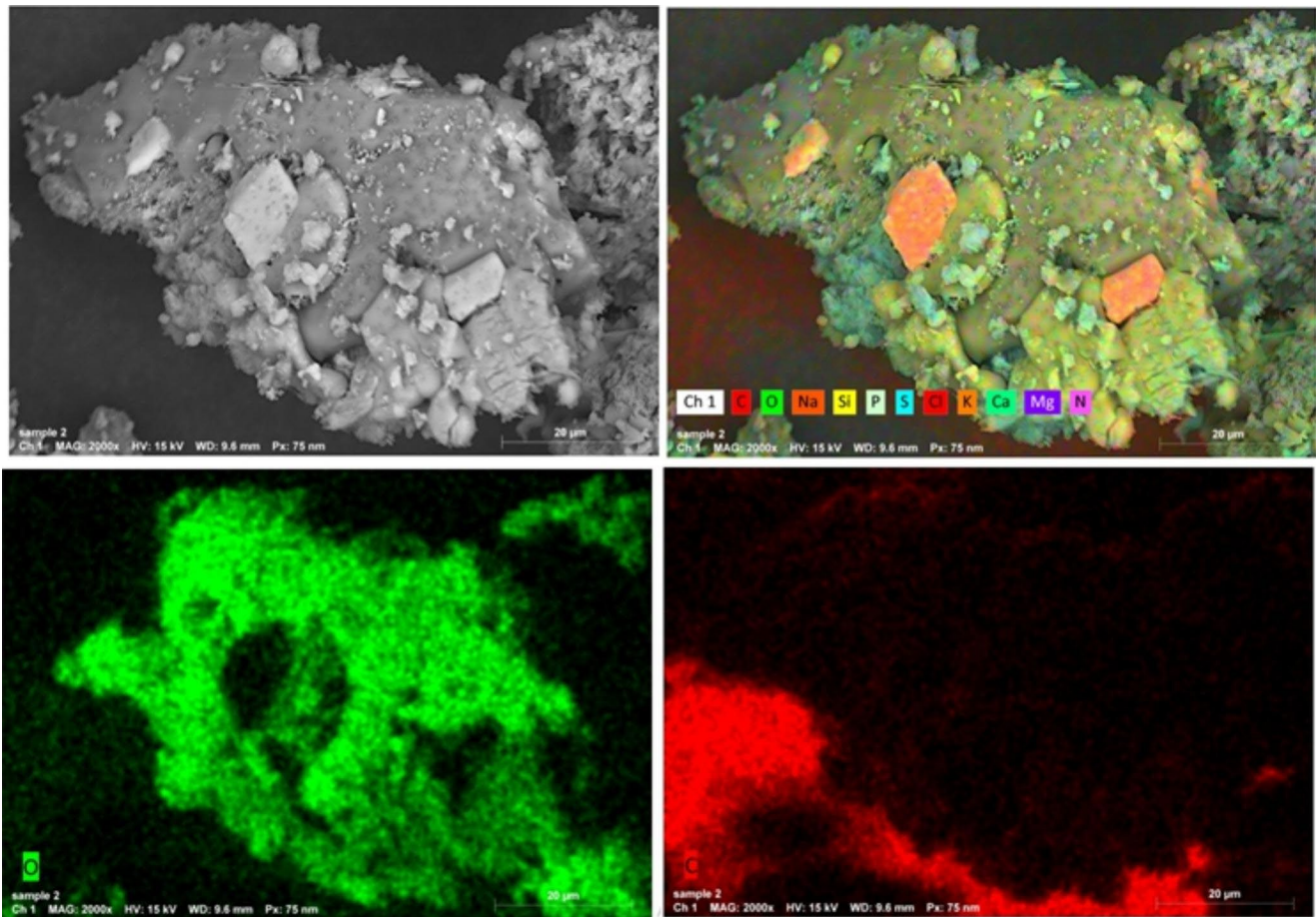


**Fig. 5** SEM/EDX mapping analysis for the synthesized CNCs

**Table 2** The Box-Behnken design results with actual and predicted data of Sr sorption capacity by microbial CNCs

Factors Runs	contact time (min.)	Factors Sr <sup>2+</sup> conc. (ppm)	CNCs wt. (g)	Response	
				Sr <sup>2+</sup> sorption capacity mg g <sup>-1</sup> dry wt	
				Actual	Predicted
1	15.0	50	0.125	11.27	13.28
2	120.0	50	0.125	11.53	18.57
3	15.0	500	0.125	58.63	51.58
4	120.0	500	0.125	58.29	82.84
5	15.0	275	0.050	156.25	149.59
6	120.0	275	0.050	281.89	243.63
7	15.0	275	0.200	30.96	69.21
8	120.0	275	0.200	31.61	38.27
9	67.5	50	0.050	58.27	89.48
10	67.5	500	0.050	186.33	200.02
11	67.5	50	0.200	6.28	7.41
12	67.5	500	0.200	42.39	11.17
13	67.5	275	0.125	48.66	48.49
14	67.5	275	0.125	48.32	48.49

**Table 3** Analysis of variance (ANOVA) of experimental data for Sr<sup>2+</sup> adsorption

Source	DF	Adj SS	Adj MS	T value	F Value	P Value
Model	9	5846.42	649.60		16.69	0.008
Linear	3	5334.32	1778.11		45.68	0.001
Contact time min.	1	179.46	179.46	1.09	4.61	0.098
Sr <sup>2+</sup> conc. ppm	1	4058.10	4058.10	2.24	104.26	0.001
CNCs wt. g	1	1096.76	1096.76	-4.96	28.18	0.006
Square	3	40.00	13.33		0.34	0.797
Contact time . *contact time .	1	4.95	4.95	0.84	0.13	0.739
Sr <sup>2+</sup> conc. *Sr <sup>2+</sup> conc.	1	28.68	28.68	-1.44	0.74	0.439
CNCs wt. *CNCs wt.	1	0.33	0.33	2.53	0.01	0.931
2-Way Interaction	3	472.10	157.37		4.04	0.105
Contact time *Sr <sup>2+</sup> conc.	1	1.42	1.42	-0.01	0.04	0.858
Contact time *CNCs wt.	1	263.90	263.90	-1.53	6.78	0.060
Sr conc. ppm *CNCs wt.	1	206.78	206.78	-1.13	5.31	0.082
Error	4	155.69	38.92			
Lack-of-Fit	3	155.69	51.90		12813.82	0.006
Pure Error	1	0.00	0.00			
Total	13	6002.11				

**R<sup>2</sup> = 97.41%, R<sup>2</sup>(adj) 91.57%**

The analysis of variance (ANOVA) was applied at 95% confidence intervals; variables and models would be statistically considerable at levels of significance, *P* value < 0.05. (-) *T* value indicates negative effect, (+) *T* value indicates positive effect  
 DF: degree of freedom, adj SS: adjusted sum of squares, adj MS: adjusted mean of squares, *F* Value: ratio of two variance, *P* Value: probability value, R<sup>2</sup>: determination coefficient, R<sup>2</sup>(adj): adjusted determination coefficient

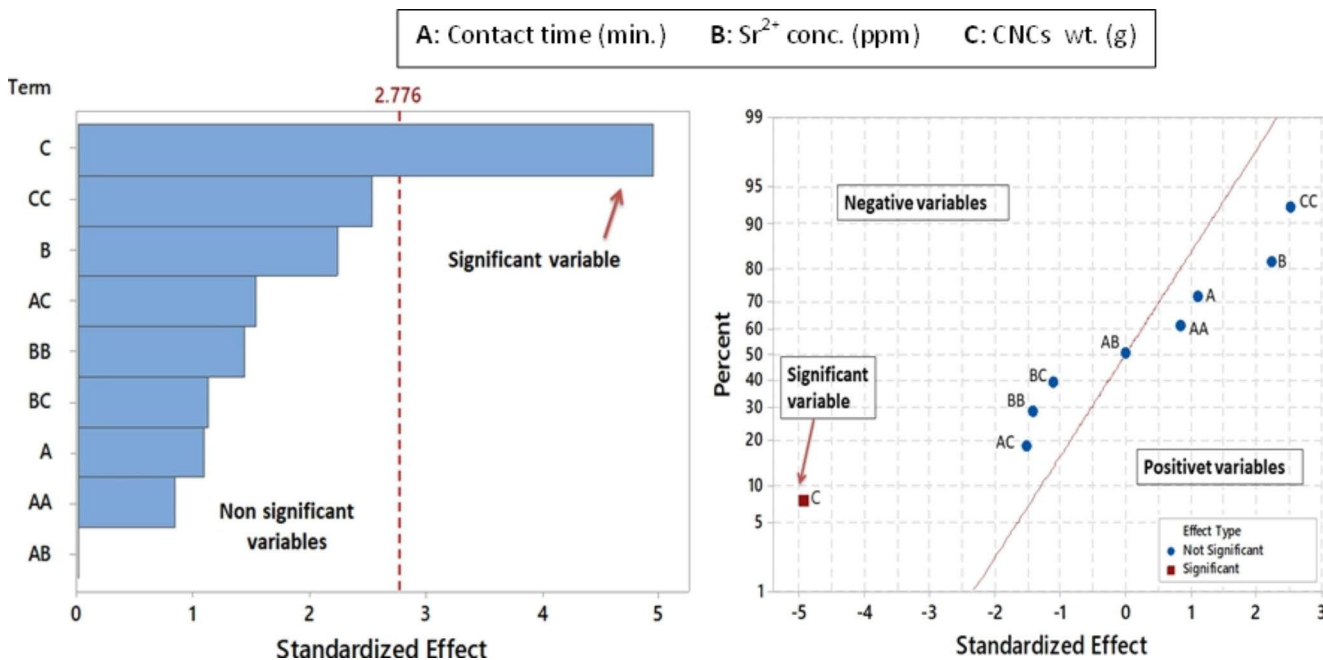


**Fig. 6** Graphical demonstrations for Sr<sup>2+</sup> sorption capacity results obtained from the BBD. (a) Pareto chart showing the significance of effect for each tested variable. (b) Normal plot showing the positively and negatively affecting variables on sorption capacity

**The Significance of Variables**

The Pareto chart identifies the most critical factor in the removal process by indicating whether or not the factors are statistically significant. The reference line is indicated by the perpendicular red dashed line in (Fig. 6a). The effects are statistically significant if they fall next to the reference line on the right. (Fig. 6a) shows that only the weight of the CNCs is statistically significant,

whereas the other components are not. The normal pareto in Fig. 6b illustrated the positive and negative effects of all variables on the response. While the estimated effect of an important factor will often be moved considerably off the zero-line, the estimated effect of an unimportant factor will typically be on or close to the near-zero line.

## Validation of Assumption

The graph of residuals and fit shown in (Fig. 7) could be used to confirm the distribution's necessary assumptions, such as randomness and constant variance of residuals. The model adhered to the provided assumptions because the residuals were scattered with random locations on either side of the zero line and did not follow any discernible pattern.

The hypothesis that the residuals were independent of one another could be confirmed using the residual versus order plot for the strontium process shown in (Fig. 7d). The fact that the residuals in time order showed no pattern and fell randomly around the center line for both adsorbents suggested that they were unrelated to one another. The normal probability plot could be used to verify if the residuals were distributed normally. (Fig. 7a) shows the typical plot of the residuals for the removal of strontium using CNCs. The residuals displayed a nearly straight line, indicating that they met the normality assumption.

## Optimization of Response

The optimization plot shows how various variables affect the expected results. It identifies the best predictive

parameters for the variables as well as the point estimate and prediction range of the responses. (Fig. 8) shows response optimization plots of strontium sorption capacity using CNCs. The objective of this study was to maximize the removal of  $\text{Sr}^{2+}$  and the sorption capacity. The response optimizer predicts that the maximum sorption capacity of  $\text{Sr}^{2+}$  for CNCs (266.8602 mg/g dry weight.) could be achieved with a desirability of 94.547% with the following conditions: contact time = 120 min, initial  $\text{Sr}^{2+}$  conc. = 463.636 ppm and CNCs weight = 0.050 g.

## Three-dimensional and Two-dimensional Response Surface

The ideal points, the impact of each variable, and how they interacted during the optimization processes were all identified by surveying the 2D contour plots and 3D surface [77, 78]. It gave the impression of a two-dimensional picture by connecting all spots with similar responses to contour lines that produce constant responses. The plot consisted of three distinct components: (a) predictors on the x- and y-axes, (b) a contour line connecting points with the same response, and (c) contour bands of the same color denoting ranges of the response variable. The link between different parameters

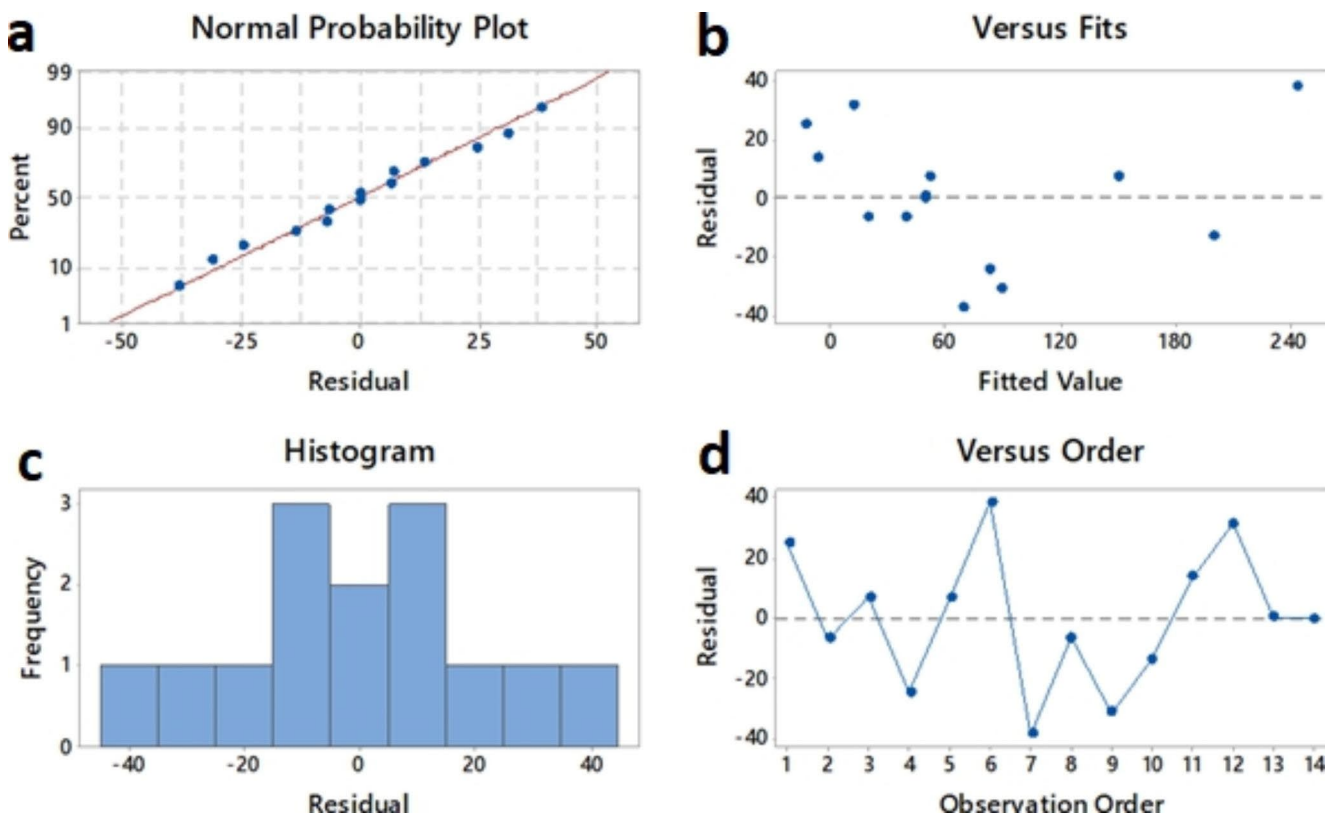


**Fig. 7** Validation of assumption (a) Normal plots of residuals for  $\text{Sr}^{2+}$  sorption capacity (b) Residual vs. fit plots of  $\text{Sr}^{2+}$  sorption capacity (c) Histogram of residual (d) Residual vs. order plot of  $\text{Sr}^{2+}$  sorption capacity

**Fig. 8** Response optimization plots of Sr<sup>2+</sup> sorption capacity using microbial CNCs

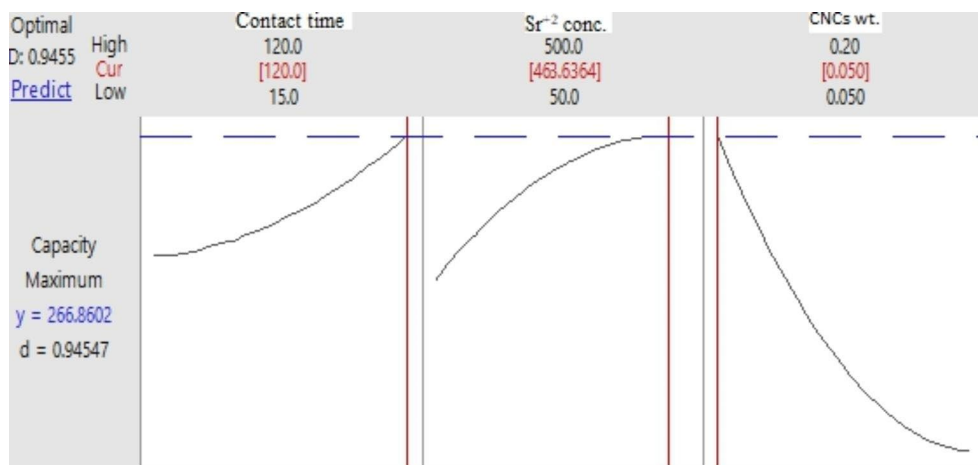


**Fig. 9** Response surface plot for (A, a) interaction of initial Sr<sup>2+</sup> concentration and CNCs weight, (B, b) interaction of Sr<sup>2+</sup> concentration and contact time and (C, c) interaction of CNCs weight and contact time

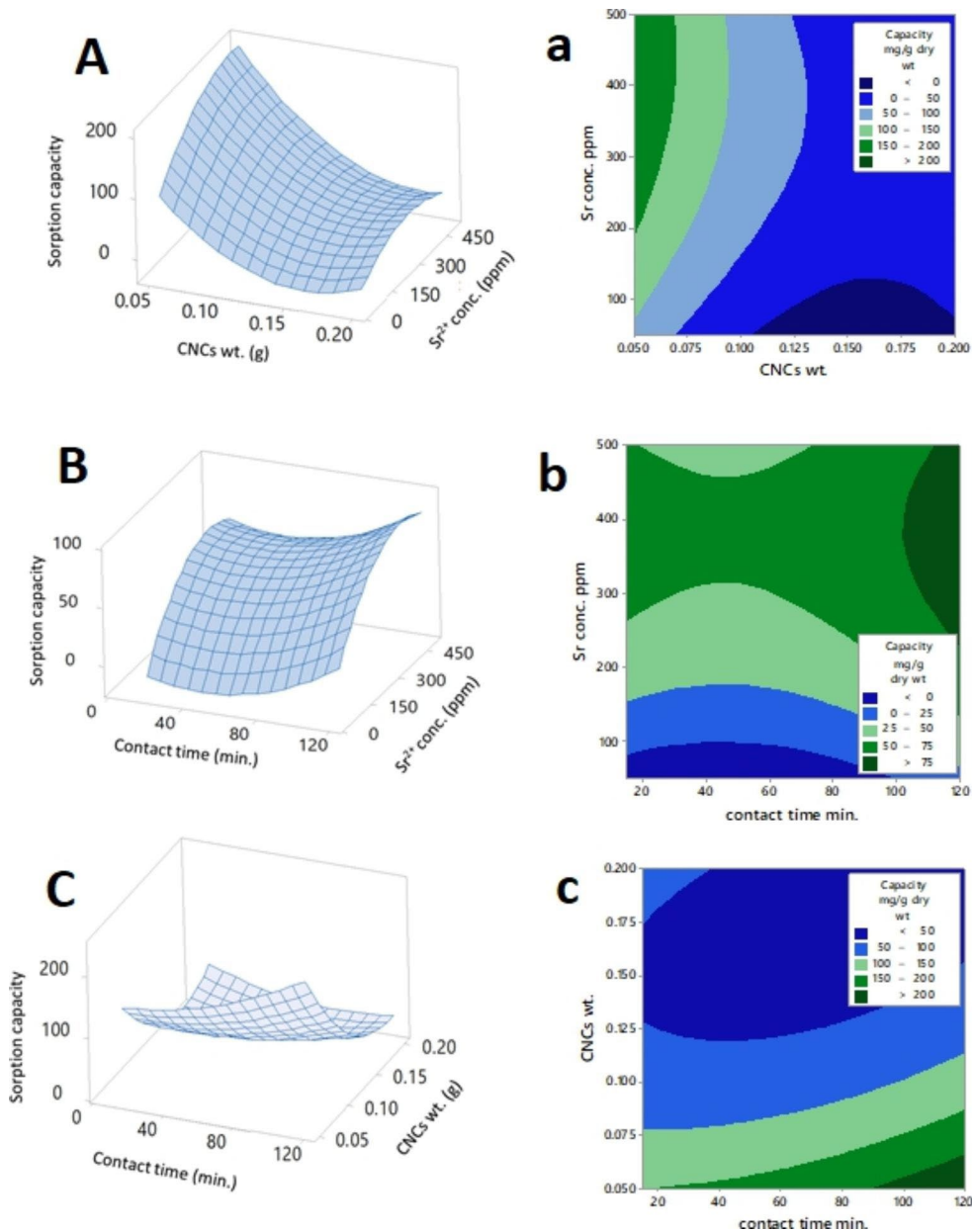


**Table 4** A comparison of maximum Sr<sup>2+</sup> adsorption capacity of several adsorbents with CNCs

Adsorbent	pH	sorption capacity mg g <sup>-1</sup> dry wt	References
Titanate nanofibers	7.0	55.20	(Wang et al. 2009)
Carboxymethylated cellulose	4.0	108.7	(Shawabkeh et al. 2002)
Composite magnetic nanoparticles	10.25	23	(Tu et al. 2016)
Carbon nanotubes	7.0	6.62	(Yavari et al. 2010)
Hydroxyapatite nanoparticles	7.0	50.47	(Borrok and Fein 2005)
Carboxymethylated chitosan	4.0	99.0	(Park et al. 2010)
Potassium tetratitanate whisker	6.0	104.2	(Jianlong 2002)
Nanocrystalline cellulose	5.0	266	This study

Borrok DM, Fein JB (2005) The impact of ionic strength on the adsorption of protons, Pb, Cd, and Sr onto the surfaces of Gram negative bacteria: testing non-electrostatic, diffuse, and triple-layer models. *Journal of colloid and interface science* 286:110–126

Jianlong W (2002) Biosorption of copper (II) by chemically modified biomass of *Saccharomyces cerevisiae*. *Process Biochemistry* 37:847–850

Park Y, Lee Y-C, Shin WS, Choi S-J (2010) Removal of cobalt, strontium and cesium from radioactive laundry wastewater by ammonium molybdophosphate–polyacrylonitrile (AMP–PAN). *Chemical Engineering Journal* 162:685–695

Shawabkeh RA, Rockstraw DA, Bhada RK (2002) Copper and strontium adsorption by a novel carbon material manufactured from pecan shells. *Carbon* 40:781–786

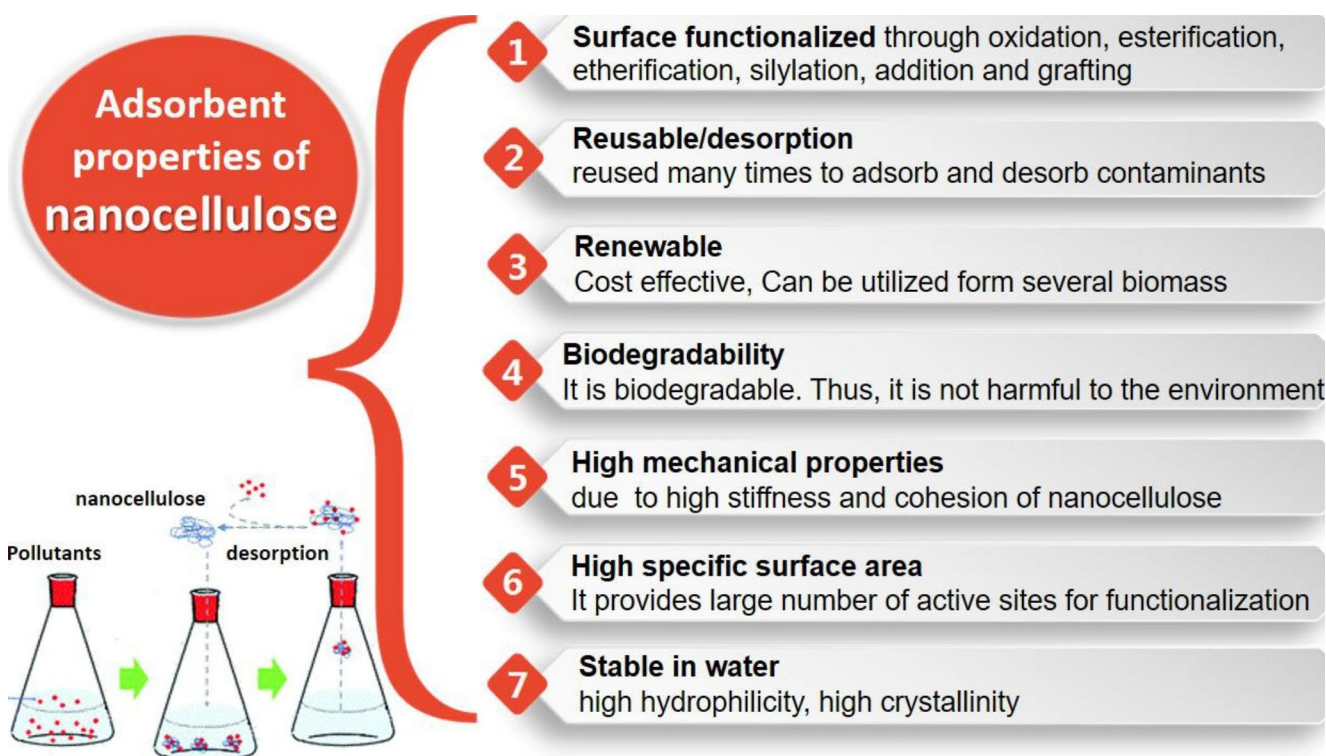
Tu Y-J, You C-F, Zhang Z, Duan Y, Fu J, Xu D (2016) Strontium removal in seawater by means of composite magnetic nanoparticles derived from industrial sludge. *Water* 8:357

Wang M, Xu L, Peng J, Zhai M, Li J, Wei G (2009) Adsorption and desorption of Sr (II) ions in the gels based on polysaccharide derivatives. *Journal of Hazardous Materials* 171:820–826

Yavari R, Huang Y, Mostofizadeh A (2010) Sorption of strontium ions from aqueous solutions by oxidized multiwall carbon nanotubes. *Journal of Radioanalytical and Nuclear Chemistry* 285:703–710

(contact length, initial concentration, and CNCs weight) was used to remove strontium from wastewater, and the amount of strontium removed was indicated by the contour plot in (Fig. 9a,b,c). The graph's lighter sections

showed lower removal processes, which was undesirable, while the darker region indicated higher removal. Figure 7 (A, a) represents the interaction between the initial Sr<sup>2+</sup> concentration and the CNC's weight on the sorption

**Fig. 10** Various characteristics of nanocellulose related to adsorbent properties

capacity. Where the interaction between  $\text{Sr}^{2+}$  concentration and contact time was shown in Fig. 7 (B, b). Furthermore, the interaction between CNCs weight and contact time is shown in Fig. 7 (C, c).

### Comparison of the $\text{Sr}^{2+}$ Adsorption Capacity with Other Adsorbents

The removal of  $\text{Sr}^{2+}$  from the CNC's sorption capacity was compared to that of other adsorbents in Table 4. As demonstrated in Table 4, the greatest amount of  $\text{Sr}^{2+}$  that could be adsorbed on the CNCs was 266 mg  $\text{Sr}^{2+}$ /g dry wt. This adsorption capacity was higher than that of a majority of the adsorbents.

Nanocellulose, as an adsorbent material, has various amazing properties and hence has the potential to be used in real applications for effective water treatment. (Fig. 10) outlines the significance of these unique properties of nanocellulose in its use as an adsorbent [79–82].

### Conclusion

This study focused on the adsorption process studies to optimize and maximize the removal of  $\text{Sr}^{2+}$  from aqueous solution using microbial CNCs. *Neurospora intermedia* was effectively used to biosynthesize CNC, which was then used as an adsorbate. The relationship between the variables and the sorbent's adsorption capacity was examined using RSM based on three-variable BBD. The experimentally determined values and the values predicted by the model for the response variable agreed well ( $R^2=0.9741$ ,  $R^2_{\text{adj}} 0.9157$ ). The contact time, initial  $\text{Sr}^{2+}$  concentration, and CNC weight were determined to be the best sorption conditions for effectively removing  $\text{Sr}^{2+}$ . The highest dynamic adsorption capacity of  $\text{Sr}^{2+}$  ions was determined to be 281.89 mg/g dry wt under these optimal conditions.

**Acknowledgements** The authors express their appreciation to Dr. Mahmoud A. Mosleh, Nuclear Metallurgy Department, Egyptian Atomic Energy Authority (EAEA) and Dr. Amira G. Zaki Plant Research Department, Nuclear Research Center, Egyptian Atomic Energy Authority (EAEA), for their continuous support and assistance in reviewing and revising the manuscript. The authors are greatly thankful to Dr. Gharieb S. El-Sayyad, Drug Radiation Research Department, Egyptian Atomic Energy Authority (EAEA) and Dr. Ali Maged Geology Department, Faculty of Science, Suez University, Egypt, for assistance in the SEM-EDX and BET analysis, respectively.

**Author Contributions** RSA suggested the research point, investigated the article, conceived and designed the research, conducted experimental methodology and provided the used chemicals. MKM conceived and designed the research, conducted experimental methodology, participated in data analysis and representation. YAH conceived and designed research, conducted experimental methodology, provided a

practical guidance, wrote the original-draft, and participated in manuscript revising and editing. EMK conducted experimental methodology, participated in data analysis and representation. All authors read and approved the article.

**Funding** No fund.

Open access funding provided by The Science, Technology & Innovation Funding Authority (STDF) in cooperation with The Egyptian Knowledge Bank (EKB).

**Data Availability** Data will be made available on request.

### Declarations

**Competing Interests** The authors declare that they have no competing interest.

**Ethical Approval** Not applicable.

**Open Access** This article is licensed under a Creative Commons Attribution 4.0 International License, which permits use, sharing, adaptation, distribution and reproduction in any medium or format, as long as you give appropriate credit to the original author(s) and the source, provide a link to the Creative Commons licence, and indicate if changes were made. The images or other third party material in this article are included in the article's Creative Commons licence, unless indicated otherwise in a credit line to the material. If material is not included in the article's Creative Commons licence and your intended use is not permitted by statutory regulation or exceeds the permitted use, you will need to obtain permission directly from the copyright holder. To view a copy of this licence, visit <http://creativecommons.org/licenses/by/4.0/>.

### References

- Zhang, L., et al., *Adsorption characteristics of strontium on synthesized antimony silicate*. Chemical Engineering Journal, 2015. 277: p. 378–387.
- Mu, W., et al., *Efficient removal of Cs + and Sr2 + from aqueous solution using hierarchically structured hexagonal tungsten trioxide coated Fe3O4*. Chemical Engineering Journal, 2017. 319: p. 170–178.
- Dahl, S., et al., *Incorporation and distribution of strontium in bone*. Bone, 2001. 28(4): p. 446–453.
- Mangano, J.J. and J.D. Sherman, *Elevated in vivo strontium-90 from nuclear weapons test fallout among cancer decedents: a case-control study of deciduous teeth*. International Journal of Health Services, 2011. 41(1): p. 137–158.
- Ma, B., et al., *Removal of Co2+, Sr2 + and Cs + from aqueous solution by phosphate-modified montmorillonite (PMM)*. Desalination, 2011. 276(1–3): p. 336–346.
- Ambashta, R.D. and M.E. Sillanpää, *Membrane purification in radioactive waste management: a short review*. Journal of environmental radioactivity, 2012. 105: p. 76–84.
- Amata, R., et al., *Toxicological profile for strontium 2004*.
- Ryu, J., et al., *Strontium ion (Sr2+) separation from seawater by hydrothermally structured titanate nanotubes: Removal vs. recovery*. Chemical Engineering Journal, 2016. 304: p. 503–510.
- Nur, T., et al., *Removal of strontium from aqueous solutions and synthetic seawater using resorcinol formaldehyde polycondensate resin*. Desalination, 2017. 420: p. 283–291.

10. Zhang, L., et al., *Strontium (II) adsorption on Sb (III)/Sb<sub>2</sub>O<sub>5</sub>*. Chemical Engineering Journal, 2015. 267: p. 245–252.
11. Raut, D., P. Mohapatra, and V. Manchanda, *A highly efficient supported liquid membrane system for selective strontium separation leading to radioactive waste remediation*. Journal of membrane science, 2012. 390: p. 76–83.
12. Faghihian, H., et al., *Preparation of a novel PAN–zeolite nanocomposite for removal of Cs + and Sr<sup>2+</sup> from aqueous solutions: Kinetic, equilibrium, and thermodynamic studies*. Chemical engineering journal, 2013. 222: p. 41–48.
13. Fu, F. and Q. Wang, *Removal of heavy metal ions from wastewaters: a review*. Journal of environmental management, 2011. 92(3): p. 407–418.
14. Shen, C., et al., *Global profile of heavy metals and semimetals adsorption using drinking water treatment residual*. Chemical Engineering Journal, 2019. 372: p. 1019–1027.
15. Hasanien, Y.A., et al., *Molecular identification and evaluation of gamma irradiation effect on modulating heavy metals tolerance in some of novel endophytic fungal strains*. Archives of Microbiology, 2021. 203: p. 4867–4878.
16. Bolisetty, S., M. Peydayesh, and R. Mezzenga, *Sustainable technologies for water purification from heavy metals: review and analysis*. Chemical Society Reviews, 2019. 48(2): p. 463–487.
17. Mahfoudhi, N. and S. Boufi, *Nanocellulose as a novel nanostructured adsorbent for environmental remediation: a review*. Cellulose, 2017. 24(3): p. 1171–1197.
18. Rasalingam, S., R. Peng, and R.T. Koodali, *Removal of hazardous pollutants from wastewaters: applications of TiO<sub>2</sub>-SiO<sub>2</sub> mixed oxide materials* Journal of Nanomaterials, 2014. 2014.
19. Jordan, J.H., M.W. Easson, and B.D. Condon, *Alkali hydrolysis of sulfated cellulose nanocrystals: optimization of reaction conditions and tailored surface charge*. Nanomaterials, 2019. 9(9): p. 1232.
20. Garba, Z.N., et al., *Microcrystalline cellulose (MCC) based materials as emerging adsorbents for the removal of dyes and heavy metals—a review*. Science of the Total Environment, 2020. 717: p. 135070.
21. Walling, B., et al., *Bacterial nanocellulose: A novel nanostructured bio-adsorbent for green remediation technology*. Acta Ecologica Sinica, 2023.
22. Jin, H., et al., *Superhydrophobic and superoleophobic nanocellulose aerogel membranes as bioinspired cargo carriers on water and oil*. Langmuir, 2011. 27(5): p. 1930–1934.
23. Banza, M. and H. Rutto, *Selective removal of Cr (VI) from hydro-metallurgical effluent using modified cellulose nanocrystals (CNCs) with succinic anhydride and ethylenediaminetetraacetic acid: Isotherm, kinetics, and thermodynamic studies*. The Canadian Journal of Chemical Engineering, 2023. 101(2): p. 896–908.
24. Banza, M. and H. Rutto, *Modelling of adsorption of nickel (II) by blend hydrogels (cellulose nanocrystals and corn starch) from aqueous solution using adaptive neuro-fuzzy inference systems (ANFIS) and artificial neural networks (ANN)*. The Canadian Journal of Chemical Engineering, 2023. 101(4): p. 1906–1918.
25. Sharma, P.R., et al., *Nanocellulose from spinifex as an effective adsorbent to remove cadmium (II) from water*. ACS Sustainable Chemistry & Engineering, 2018. 6(3): p. 3279–3290.
26. Si, R., et al., *Nanocellulose Based Adsorbents for Heavy Metal Ions Removal 2021*.
27. Ahmad, N., et al., *Rapid synthesis of silver nanoparticles using dried medicinal plant of basil*. Colloids and Surfaces B: Biointerfaces, 2010. 81(1): p. 81–86.
28. Khandel, P. and S.K. Shahi, *Mycogenic nanoparticles and their bio-prospective applications: current status and future challenges*. Journal of Nanostructure in Chemistry, 2018. 8(4): p. 369–391.
29. Banza, M. and H. Rutto, *Extraction of cellulose nanocrystals from millet (Eleusine coracana) husk waste: optimization using Box Behnken design in response surface methodology (RSM)*. International Nano Letters, 2022. 12(3): p. 257–272.
30. Hasanien, Y.A., et al., *Optimization, purification, and structure elucidation of anthraquinone pigment derivative from Talaromyces purpureogenus as a novel promising antioxidant, anticancer, and kidney radio-imaging agent*. Journal of Biotechnology, 2022. 356: p. 30–41.
31. Kabuba, J. and M. Banza, 2020. *Ion-exchange process for the removal of Ni (II) and Co (II) from wastewater using modified clinoptilolite: modeling by response surface methodology and artificial neural network* Results in Engineering, 2020. 8: p. 100189.
32. Singh, S., J.P. Chakraborty, and M.K. Mondal, *Optimization of process parameters for torrefaction of Acacia nilotica using response surface methodology and characteristics of torrefied biomass as upgraded fuel*. Energy, 2019. 186: p. 115865.
33. Liao, Q. and G. Lin, *Reduced basis ANOVA methods for partial differential equations with high-dimensional random inputs*. Journal of Computational Physics, 2016. 317: p. 148–164.
34. Helal, G., et al., *Studies on cellulases of some cellulose-degrading soil fungi*. Archives of Microbiology, 2022. 204(1): p. 1–16.
35. Çolak, A. and M. Bicici, *PCR detection of Fusarium oxysporum f. sp. radicis-lycopersici and races of F. oxysporum f. sp. lycopersici of tomato in protected tomato-growing areas of the eastern Mediterranean region of Turkey*. Turkish Journal of Agriculture and Forestry, 2013. 37(4): p. 457–467.
36. Dox, A.W., *The intracellular enzymes of penicillium and aspergillus: with special reference to those of Penicillium camemberti*. Vol. 120. 1910: US Department of Agriculture, Bureau of Animal Industry.
37. Bai, W., J. Holbery, and K. Li, *A technique for production of nanocrystalline cellulose with a narrow size distribution*. Cellulose, 2009. 16(3): p. 455–465.
38. Satyamurthy, P., et al., *Preparation and characterization of cellulose nanowhiskers from cotton fibres by controlled microbial hydrolysis*. Carbohydrate Polymers, 2011. 83(1): p. 122–129.
39. Soliman, I.A., et al., *Irradiation impact on biological activities of Anthraquinone pigment produced from Talaromyces purpureogenus and its evaluation, characterization and application in beef burger as natural preservative*. BMC microbiology, 2022. 22(1): p. 325.
40. Dutta, H., *Potential of Polysaccharide Nanoparticles in Foods, in Nanotechnology Horizons in Food Process Engineering*. 2023, Apple Academic Press. p. 85–155.
41. Zaki, A.G., Y.A. Hasanien, and G.S. El-Sayyad, *Novel fabrication of SiO<sub>2</sub>/Ag nanocomposite by gamma irradiated Fusarium oxysporum to combat Ralstonia solanacearum*. AMB Express, 2022. 12(1): p. 1–18.
42. Nilsson, C., *Preparation and characterization of nanocellulose from wheat bran 2017*.
43. Ling, Z., et al., *Effects of ball milling on the structure of cotton cellulose*. Cellulose, 2019. 26: p. 305–328.
44. Bano, S. and Y.S. Negi, *Studies on cellulose nanocrystals isolated from groundnut shells*. Carbohydrate polymers, 2017. 157: p. 1041–1049.
45. Sulaiman, N.S., et al., *Optimization of activated carbon preparation from cassava stem using response surface methodology on surface area and yield*. Journal of Cleaner Production, 2018. 198: p. 1422–1430.
46. Dehghani, M.H., et al., *Optimization of fluoride adsorption onto natural and modified pumice using response surface methodology: isotherm, kinetic and thermodynamic studies*. Korean Journal of Chemical Engineering, 2017. 34(2): p. 454–462.



47. Faraji, M., et al., *Optimizing the removal of humic acid with poly-aluminum chloride and polyaluminum ferric chloride as green coagulants using response surface methodology*. Desalination and Water Treatment, 2019. 139: p. 297–304.
48. Bazrafshan, E., et al., *Photocatalytic degradation of catechol using ZnO nanoparticles as catalyst: Optimizing the experimental parameters using the Box-Behnken statistical methodology and kinetic studies*. Microchemical Journal, 2019. 147: p. 643–653.
49. Joudeh, N. and D. Linke, *Nanoparticle classification, physico-chemical properties, characterization, and applications: a comprehensive review for biologists*. Journal of Nanobiotechnology, 2022. 20(1): p. 1–29.
50. Shaheen, T.I., S. Salem, and A. Fouda, *Current advances in fungal nanobiotechnology: mycofabrication and applications*. Microbial Nanobiotechnology, 2021: p. 113–143.
51. Xu, P., et al., *Facile fabrication of silver nanoparticles deposited cellulose microfibril nanocomposites for catalytic application*. Journal of colloid and interface science, 2018. 526: p. 194–200.
52. Orelma, H., et al., *Optical cellulose fiber made from regenerated cellulose and cellulose acetate for water sensor applications*. Cellulose, 2020. 27(3): p. 1543–1553.
53. Simão, C.D., et al., *Optical and mechanical properties of nanofibrillated cellulose: Toward a robust platform for next-generation green technologies*. Carbohydrate polymers, 2015. 126: p. 40–46.
54. Islam, M.S., et al., *Potential aspect of rice husk biomass in Australia for nanocrystalline cellulose production*. Chinese Journal of Chemical Engineering, 2018. 26(3): p. 465–476.
55. Salimi, F., et al., *Optimization and characterization of eco-friendly antimicrobial nanocellulose sheet prepared using carbon dots of white mulberry (Morus alba L.)*. Journal of the Science of Food and Agriculture, 2021. 101(8): p. 3439–3447.
56. Bera, B., *Nanoporous silicon prepared by vapour phase strain etch and sacrificial technique*. Int. J. Comput. Appl, 2015. 975: p. 8887.
57. Kumar, A. and C.K. Dixit, *Methods for characterization of nanoparticles*, in *Advances in nanomedicine for the delivery of therapeutic nucleic acids*. 2017, Elsevier. p. 43–58.
58. Khayata, N., et al., *Preparation of vitamin E loaded nanocapsules by the nanoprecipitation method: From laboratory scale to large scale using a membrane contactor*. International journal of pharmaceuticals, 2012. 423(2): p. 419–427.
59. Zhang, H., et al., *Nano-size porous carbon spheres as a high-capacity anode with high initial coulombic efficiency for potassium-ion batteries*. Nanoscale horizons, 2020. 5(5): p. 895–903.
60. Dufresne, A., *Nanocellulose processing properties and potential applications*. Current Forestry Reports, 2019. 5: p. 76–89.
61. Honary, S. and F. Zahir, *Effect of zeta potential on the properties of nano-drug delivery systems-a review (Part 2)*. Tropical journal of pharmaceutical research, 2013. 12(2): p. 265–273.
62. Masruchin, N., et al. *Particle size distribution and yield analysis of different charged cellulose nanofibrils obtained by TEMPO-mediated oxidation*. in *IOP Conference Series: Earth and Environmental Science*. 2020. IOP Publishing.
63. Lu, Z., et al., *Preparation, characterization and optimization of nanocellulose whiskers by simultaneously ultrasonic wave and microwave assisted*. Bioresource technology, 2013. 146: p. 82–88.
64. Youssef, B., et al., *Preparation and properties of bionanocomposite films reinforced with nanocellulose isolated from Moroccan alfa fibres*. Autex Research Journal, 2015. 15(3): p. 164–172.
65. Lu, P. and Y.-L. Hsieh, *Preparation and properties of cellulose nanocrystals: rods, spheres, and network*. Carbohydrate polymers, 2010. 82(2): p. 329–336.
66. Socrates, G., *Infrared and Raman characteristic group frequencies: tables and charts*. 2004: John Wiley & Sons.
67. Gopakumar, D.A., et al., *Nanocellulose: Extraction and application as a sustainable material for wastewater purification*, in *New polymer nanocomposites for environmental remediation*. 2018, Elsevier. p. 469–486.
68. Modena, M.M., et al., *Nanoparticle characterization: what to measure?* Advanced Materials, 2019. 31(32): p. 1901556.
69. Adnan, S., et al. *Properties of paper incorporated with nanocellulose extracted using microbial hydrolysis assisted shear process*. in *IOP conference series: materials science and engineering*. 2018. IOP Publishing.
70. Nasihin, Z.D., et al. *Preparation of nanocellulose bioplastic with a gradation color of red and yellow*. in *IOP Conference Series: Materials Science and Engineering*. 2020. IOP Publishing.
71. Daicho, K., et al., *The crystallinity of nanocellulose: dispersion-induced disordering of the grain boundary in biologically structured cellulose*. ACS Applied Nano Materials, 2018. 1(10): p. 5774–5785.
72. Akhtar, K., et al., *Scanning electron microscopy: Principle and applications in nanomaterials characterization* Handbook of materials characterization, 2018: p. 113–145.
73. Ashour, A., et al., *Antimicrobial activity of metal-substituted cobalt ferrite nanoparticles synthesized by sol-gel technique*. Particology, 2018.
74. Mourabet, M., et al., *Removal of fluoride from aqueous solution by adsorption on hydroxyapatite (HAp) using response surface methodology*. Journal of Saudi Chemical Society, 2015. 19(6): p. 603–615.
75. Sahu, J., J. Acharya, and B. Meikap, *Optimization of production conditions for activated carbons from Tamarind wood by zinc chloride using response surface methodology*. Bioresource technology, 2010. 101(6): p. 1974–1982.
76. Le Man, H., S. Behera, and H. Park, *Optimization of operational parameters for ethanol production from Korean food waste leachate*. International Journal of Environmental Science & Technology, 2010. 7(1): p. 157–164.
77. Amiri, S., M. Reza Sohrabi, and F. Motiee, *Optimization Removal of the Ceftriaxone Drug from Aqueous Media with Novel Zero-Valent Iron Supported on Doped Strontium Hexaferrite Nanoparticles by Response Surface Methodology* ChemistrySelect, 2020. 5(19): p. 5831–5840.
78. Zaki, A.G., Y.A. Hasanien, and A.S. Abdel-Razek, *Biosorption optimization of lead (II) and cadmium (II) ions by two novel nanosilica-immobilized fungal mutants*. Journal of Applied Microbiology, 2022. 133(2): p. 987–1000.
79. Mo, L., et al., *3D multi-wall perforated nanocellulose-based polyethylenimine aerogels for ultrahigh efficient and reversible removal of Cu (II) ions from water*. Chemical Engineering Journal, 2019. 378: p. 122157.
80. Norraahim, M.N.F., et al., *Nanocellulose: A bioadsorbent for chemical contaminant remediation*. RSC advances, 2021. 11(13): p. 7347–7368.
81. Ibrahim, H., et al., *Nano-structured cellulose as green adsorbents for water purification: a mini review*. Journal of Applied Membrane Science & Technology, 2019. 23(2).
82. Voisin, H., et al., *Nanocellulose-based materials for water purification*. Nanomaterials, 2017. 7(3): p. 57.

**Publisher's Note** Springer Nature remains neutral with regard to jurisdictional claims in published maps and institutional affiliations.

Springer Nature or its licensor (e.g. a society or other partner) holds exclusive rights to this article under a publishing agreement with the author(s) or other rightsholder(s); author self-archiving of the accepted manuscript version of this article is solely governed by the terms of such publishing agreement and applicable law.